Letter

Ballistic deposition with memory: A new universality class of surface growth with a new scaling law

Ahmed Roman [1], Ruomin Zhu,[2] and Ilya Nemenman [1,3,4]
[1]*Department of Physics, Emory University, Atlanta, Georgia 30322, USA*
[2]*School of Physics, The University of Sydney, Sydney, New South Wales, Australia*
[3]*Department of Biology, Emory University, Atlanta, Georgia 30322, USA*
[4]*Initiative for Theory and Modeling of Living Systems, Emory University, Atlanta, Georgia 30322, USA*

(Received 7 March 2022; revised 23 April 2024; accepted 25 June 2024; published 5 September 2024)

Motivated by recent experimental studies in microbiology, we suggest modifying the classic ballistic deposition model of surface growth, where the memory of a deposition at a site induces more depositions at that site or its neighbors. By studying the statistics of surfaces in this model, we obtain three independent critical exponents: the growth exponent $\beta = 5/4$, the roughening exponent $\alpha = 2$, and the new (size) exponent $\gamma = 1/2$. The model requires modifying the Family-Vicsek scaling, resulting in the dynamical exponent $z = \frac{\alpha+\gamma}{\beta} = 2$. This modified scaling collapses the surface width vs time curves for various lattice sizes. This previously unobserved universality class of surface growth could describe the surface properties of a wide range of natural systems.

DOI: 10.1103/PhysRevResearch.6.L032053

Introduction. Interface growth and its roughening is a paradigmatic nonequilibrium statistical physics process with many applications [1]. Analytical, computational, and experimental studies have shown that the statistics of interface roughness in such processes usually is characterized by one of the well-known universality classes: Poisson, Edwards-Wilkinson (EW), and Kardar-Parisi-Zhang (KPZ) [2,3], as well as their extensions to quenched disorder, correlated noise, and so on [4,5]. In the first, interface heights at every point are uncorrelated. In the second, peaks in the interface are smoothed through diffusion. Finally, in the third, nearby sites in the interface help each other grow, resulting in a nonlinear amplification of fluctuations. Competition between the smoothing and the nonlinearity leads to the interface roughness that increases with time and eventually saturates at a system-size-dependent value.

More concretely, we denote the height of a one-dimensional (1D) interface at point x at time t by $h(x,t)$. Then the standard deviation of the interface height defines the interface roughness

$$w(L,t) = \overline{[[h(x,t) - \overline{h}(t)]^2]}^{1/2}, \tag{1}$$

and the average $\overline{\cdots}$ is over a domain of size L for a single realization of the interface. Such growth processes are generally characterized by three critical exponents: β, the *growth* exponent, which measures how the roughness grows with time; α, the *roughness* exponent, which parameterizes the dependence of the steady-state roughness on the system size; and z, the dynamical exponent, which relates the time at which the steady state is reached to the system size. The three exponents are related by the Family-Vicsek dynamical scaling for the interface averaged over many realizations (denoted by $\langle\cdots\rangle$) [6]:

$$\langle w(L,t)\rangle \sim L^{\alpha} f(t/L^{z}), \quad \text{with} \tag{2}$$

$$f(u) \propto \begin{cases} u^{\beta}, & u \ll 1, \\ 1, & u \gg 1, \end{cases} \tag{3}$$

which results in $z = \alpha/\beta$.

What unites all of these cases is that there is no memory or inertia in the interface growth—deposition is Markovian in time. This is a reasonable assumption when the interface is built by or from stateless agents. However, when the agents are more complex, such as when they are living cells with a multitude of internal states, such memoryless assumption should be questioned. For example, in cyclic AMP signaling in *Dictyostelium discoideum*, which is a classic biological model of collective signaling, collective motility, and development, a spreading wave of cyclic adenosine monophosphate (cAMP) activates a cell, but only if the temporal derivative of the cyclic AMP concentration is positive and large [7] [cf. Fig. 1(a)]. Thus, diffusion and degradation of cyclic AMP reduces the probability of cell activation for all cells, while cell activation events increase the probability of activation only for nearby cells. In another example, an action potential propagates in a bacterial film only if a concentration of a previously secreted extracellular potassium has not yet decayed through diffusion [8,9]. All such processes possess memory: the interface at a certain point can grow, but only if it grew here recently. The theory of such interface growth processes with memory is not yet established. In particular, we do not know the relevant critical exponents, how many different universality classes there are, and whether the Family-Viscek scaling is satisfied in such settings.

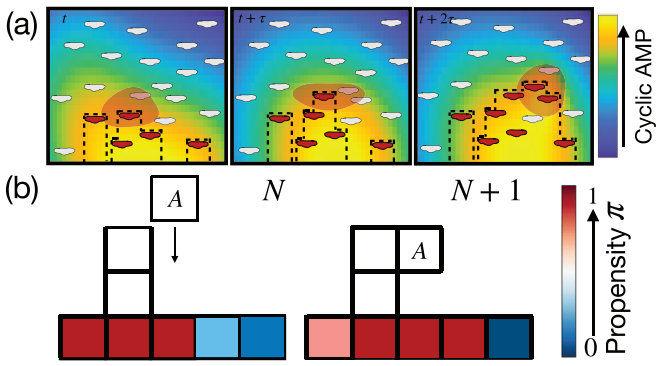

FIG. 1. (a) Three successive snapshots of the activation front (dashed lines) of model *Dictyostelium* cells. An inactive cell (white) activates (turns to red) in response to cAMP (concentration shown by the color, from blue to yellow). However, to activate, it must sense a large positive temporal change of cAMP, which exists transiently only in the pink oval-shaped region. As cAMP diffuses, only cells that are next to recently active cells can be activated. (b) A BDM model of the process. A particle A is deposited (activated) at time step N into the middle column. The propensity for deposition (shown by color) in the column and its neighbors becomes one at the next time step, while the propensity of all other sites decreases.

Here we develop a model of ballistic deposition with memory (BDM), one of the likely many possible extensions of the traditional memoryless surface growth processes, which is inspired by the microbiological systems mentioned above. We derive the critical exponents and verify them numerically. We show that the process falls into a new universality class with a new scaling law and a new scaling relation. The KPZ universality class is an unstable fixed point in the BDM dynamics. Finally, we discuss the effect of varying memory duration and show that the standard KPZ interfaces are achieved in a particular limit of the memory parameters.

Model formulation. We consider the deposition of particles on a one-dimensional substrate of length L. Each site i has a propensity value of $0 \leqslant \pi_i(N) \leqslant 1$, which determines the probability that the site will receive a particle deposition at step N. Initially, all sites are equally likely to receive a deposition; i.e., $\pi_i(0) = 1$ for all i. However, unlike in the ballistic deposition model, if a site j receives a deposition, then the propensity at that site and its nearest neighbors is set to 1 (local activation), while the propensity of all other sites is reduced by a factor r (overall degradation and diffusion), thus reducing the probability of receiving a deposition if no deposition has happened for a long time:

$$\pi_i(N+1) = \begin{cases} 1, & j-1 \leqslant i \leqslant j+1, \\ r\pi_i(N), & \text{otherwise.} \end{cases} \tag{4}$$

Overall, the probability to receive the deposition at site i at the Nth deposition event is

$$\mathcal{P}[i,N] = \frac{\pi_i(N)}{\sum_{i=1}^{L} \pi_i(N)}. \tag{5}$$

At step N, the height of the interface at site i is $h(i,N)$, with $h(i,0) = 0$. After a site i is randomly selected for the deposition according to Eq. (5), its height increases from $h(i,N)$ to

$$h(i,N+1) = \max\{h(i-1,N), h(i,N)+1, h(i+1,N)\}, \tag{6}$$

allowing for overhangs, as in the traditional ballistic deposition [cf. Fig. 1(a)]. We model the process with periodic boundary conditions, $h(L+1,N) = h(1,N)$. The dynamics of the surface and the propensity are shown in Fig. 2 for various values of r. For low values of r, a single propensity finger (the dark-blue region in the second row of Fig. 2) moves randomly, causing the deposition sites to follow a random walk, and overhangs form every time the random walk reverts. In the intermediate-r regime, multiple propensity fingers move randomly, merge, and split. These fingers induce particle depositions whose shapes are reminiscent of diffusion-limited aggregation [10], but we do not quantitatively assess this similarity here. For values of $r \approx 1$, many deposition fingers merge into a deposition front, whose fluctuation is KPZ-like (as we will discuss later), but with chasms that have a much lower height and whose frequency gets lower as $r \to 1$.

A random walker. We start with the fast-propensity decay limit, defined as $r \ll 1/L$ (see the Appendix for details). Here the probability that any site j receives a deposition at step $N+1$ given that a non-neighboring site i received a deposition at step N is

$$\sum_{\substack{j \notin \{i-1,i,i+1\} \\ 1 \leqslant j \leqslant L}} \mathcal{P}[j,N+1|i,N] = \sum_{\substack{j \notin \{i-1,i,i+1\} \\ 1 \leqslant j \leqslant L}} \frac{\pi_j(N)}{\sum_{k=1}^{L} \pi_k(N)} < \frac{Lr}{3} \ll \frac{1}{3}, \tag{7}$$

where we used the bounds $\sum_{k=1}^{L} \pi_k(N) > \sum_{k \in \{i-1,i,i+1\}} \pi_k(N) = 3$ and $\sum_{\substack{j \notin \{i-1,i,i+1\} \\ 1 \leqslant j \leqslant L}} \pi_j(N) < (L-3)r < Lr$ to bound the denominator and numerator, respectively. Therefore, the location x_N of the deposition after N steps is well approximated by a 1D random walker.

Determining the natural timescale. Classical models of interface growth, such as ballistic deposition or KPZ, measure time in units of the mean number of deposited layers, $t \sim N/L$. However, when the measure of where particles can be deposited concentrates, different relations between N, L, and t emerge [11,12].

In what follows, we use the overbar $\overline{\cdots}$ to refer to spatial averaging, and we use angled brackets $\langle \cdots \rangle$ to refer to ensemble averaging. Then, in the Appendix, we show that if $\pi_{k,j}$ is the propensity at site k and realization j, then ensemble-averaged propensity $\pi(N) \equiv \langle \pi_{k,j}(N) \rangle_{\text{ens}} \equiv \lim_{M \to \infty} \frac{1}{M} \sum_{j=1}^{M} \pi_{k,j}(N)$ is independent of the site index k and is approximated by the recursion relation

$$\pi(N+1) \approx \frac{1}{L}[(L-3)r\pi(N) + 3]. \tag{8}$$

The solution of Eq. (8) (see the Appendix) has a characteristic timescale of $N_{1/e} = \frac{1}{\ln \frac{L}{(L-3)r}} \approx \frac{1}{\ln \frac{1}{r}}$ depositions, approaching a steady-state space and ensemble-averaged propensity $\pi_* = 3[L-(L-3)r]^{-1}$. In the limit $N \gg N_{1/e}$, there are $\mathcal{O}(L\pi_*)$ sites whose probability of receiving a deposition is $\mathcal{O}(1/L\pi_*)$ (see the Appendix), while all other sites have a probability near 0 of receiving a deposition. This implies that the effective

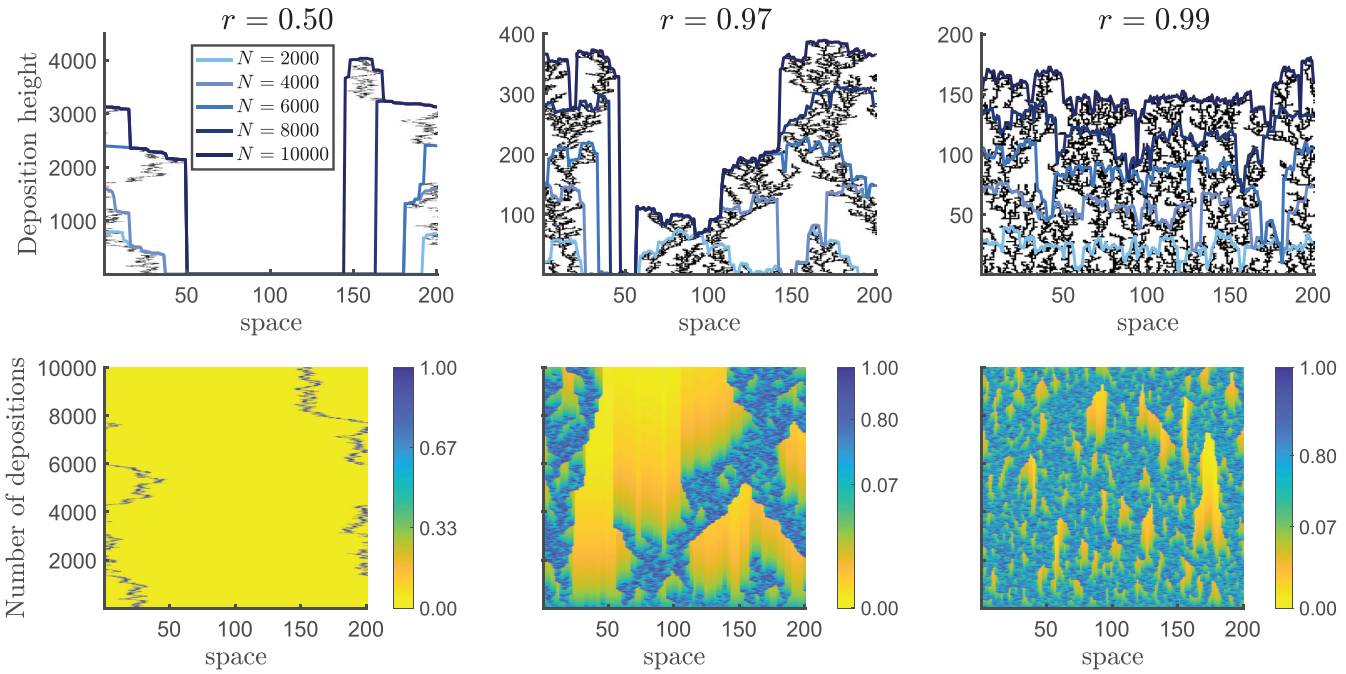

FIG. 2. Examples of the BDM interfaces. In the top row, the deposition height vs space coordinate is shown for each deposition as a black dot. Different columns are for different values of r. The blue curves show the surface height as a function of the spatial coordinate for different numbers of depositions, from $N = 2000$ (light blue) to $N = 10\,000$ (dark blue). The bottom row shows the propensity, encoded by color, as a function of space and time.

lattice length is $L\pi_*$ and motivates a definition of the number of deposited layers and, hence, a definition of time as

$$t = \eta \frac{N}{L\pi_*} = \eta\left(\frac{1}{3} - \frac{L-3}{3L}r\right)N \tag{9}$$

for any constant η. In all figures and equations, we define time as in Eq. (9) with $\eta = 1$.

Dynamical exponents. After N depositions, the deposited particles span $\mathcal{O}(\sqrt{N})$ lattice sites and the random walker has performed $\mathcal{O}(N)$ reversals, with each reversal increasing the height by 1. Thus, the space and ensemble-averaged height of the interface is $\langle \bar{h}(N)\rangle \sim c_1 \times 0 \times \frac{L-\sqrt{N}}{L} + c_2 \times N \times \frac{\sqrt{N}}{L} \sim \frac{N^{3/2}}{L} = \lambda_{r,L}^{3/2} t^{3/2}/L$ while the ensemble-averaged mean squared height is $\langle \overline{h(N)^2}\rangle \sim c_3 \times 0^2 \times \frac{L-\sqrt{N}}{L} + c_4 \times N^2 \times \frac{\sqrt{N}}{L} \sim \frac{N^{5/2}}{L} = \lambda_{r,L}^{5/2} t^{5/2}/L$ for $\lambda_{r,L} = 1/(L\pi^*)$ and some constants $c_1, \ldots, c_4$. In the above calculation, we replace $\langle \frac{1}{L}\sum_{i=1}^{L} h(i,N)\rangle^2$ by $\langle [\frac{1}{L}\sum_{i=1}^{L} h(i,N)]^2\rangle$, which we justify *a posteriori*. The resulting mean width of the interface becomes

$$\langle w(L,t)\rangle \sim \left(\lambda_{r,L}^{5/2}\frac{t^{5/2}}{L} - \delta\lambda_{r,L}^{3}\frac{t^3}{L^2}\right)^{1/2} \tag{10}$$

for some constant δ and is valid for $\sqrt{N} \ll L$.

In the regime where $\sqrt{N} \ll L$ (i.e., the random walker has yet to span the system), the width of the interface grows with time (the *growth* regime), and its value is dominated by the first term in Eq. (10):

$$\langle w(L,t)\rangle \sim \lambda_{r,L}^{5/4} t^{5/4}/\sqrt{L} \propto t^{\beta} L^{-\gamma}. \tag{11}$$

This determines the size exponent $\gamma = 1/2$ and the growth exponent $\beta = 5/4$, which are in excellent agreement with simulation values (cf. Fig. 3), despite finite-size effects, and even with r outside the regime $r \ll 1/L$.

In the regime where $\sqrt{N} \gtrsim \mathcal{O}(L)$, the random walker has spanned the lattice, and the surface roughness saturates at

$$w_{\text{sat}} \sim N^{5/4}/\sqrt{L} \sim (L^2)^{5/4}/\sqrt{L} = L^2, \tag{12}$$

This determines the roughness exponent $\alpha = 2$, which agrees with the simulations (Fig. 3).

Dynamical scaling relation and the scaling law. Since the growth and saturation regimes cross at some time t_c, it follows from Eqs. (11) and (12) that $\lambda_{r,L}^{-\beta} L^{-\gamma} t_c^{\beta} \sim L^{\alpha}$. The relation $t_c \sim \lambda_{r,L} L^{\frac{\alpha+\gamma}{\beta}} = \lambda_{r,L} L^{z}$ determines the scaling law $z = \frac{\alpha+\gamma}{\beta} = 2$ in our model. Note that $\lambda_{r,L}$ has a weak dependence on L such that for $L \gg 1$ it is essentially independent of L. The scaling relation becomes

$$\langle w(L,t)\rangle \sim L^{\alpha} f\left(t/L^{\frac{\alpha+\gamma}{\beta}}\right), \tag{13}$$

with f defined as in the Family-Vicsek scaling [6]. Indeed, plotting w/L^{α} against $t/L^{\frac{\alpha+\gamma}{\beta}}$, as in Fig. 4, collapses the width vs time curves plotted for various lattice lengths L in the inset of Fig. 4. From this, we conclude that there are three independent exponents, α, β, and γ, that fix the dynamic exponent z.

As a newly arriving particle sticks to the surface following Eq. (6), its height is either the same or larger than that of its neighbors. This introduces correlations between neighboring sites. The ensuing height fluctuations spread laterally since particles deposited at nearby sites must have an equal or larger height. This correlation length $\xi_{||}$ can only grow up to the substrate length, i.e., $\xi_{||} \sim L$ for $t \gg t_c$. Replacing L by $\xi_{||}$

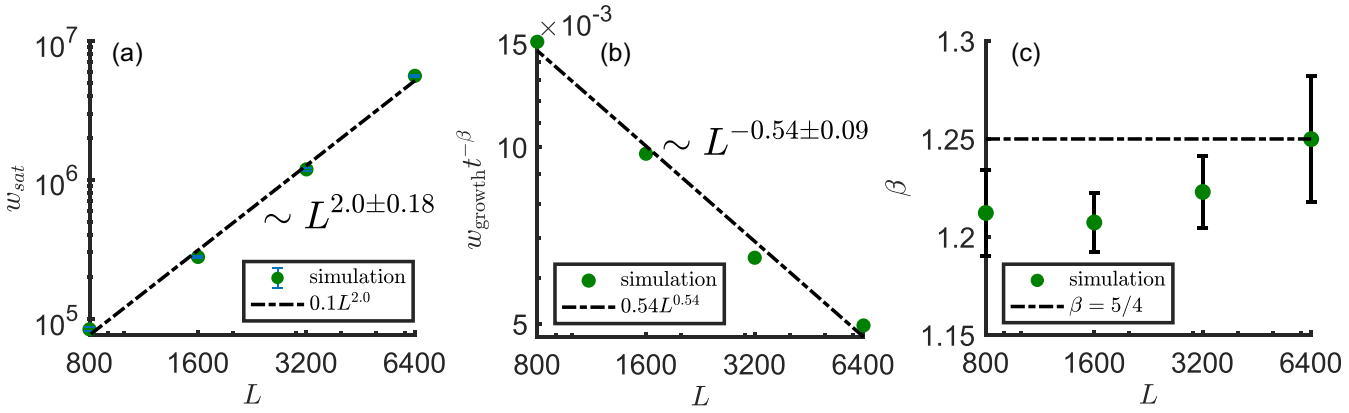

FIG. 3. (a) The saturation width of the BDM interface as a function of the system length L. The scaling L^{α}, where α is the roughening exponent, obtained from simulation, is shown. (b) The scaling of w/t^{β} in the growth regime as a function of the system size is L^{γ}; $t(N)$ is defined as in Eq. (9). The fitted scaling with the size exponent $\gamma = 0.54 \approx 0.5$ is also plotted. (c) The growth exponent β as a function of the system size L. The black dash-dotted line at $\beta = 5/4$ is the theoretical prediction, in agreement with simulations once finite-size effects become negligible. The value $r = 0.5$ is used for all subplots.

in $t_c \sim \lambda_{r,L} L^z$, we find that $\xi_{||} \sim \lambda_{r,L}^{-1/z} t_c^{1/z}$ for $t \gg t_c$. Since $\xi_{||} \sim N^{1/2}$ for $t \ll t_c$, we see that $\xi_{||} \sim \lambda_{r,L}^{-1/z} t^{1/z}$ holds for $t \ll t_c$ as well.

Varying the memory timescale. As r increases, so does the total size of the randomly moving propensity fingers $L\pi_* = \lambda_{r,L}^{-1}$. Increasing r also decreases the time to saturation t_c (cf. Fig. 5). In the limit of $r = 1$, the KPZ exponents, as seen in Fig. 5, and the standard definition of time $t = N/L$ are recovered. For most of the $r \in [0, 1]$ domain, the surface fluctuations are in the new universality class and are not in the KPZ class (cf. Fig. 5). At early times, the Poisson regime dominates the growth with a characteristic scale of $t^{1/2}$ followed by the KPZ growth with a scale of $t^{1/3}$ (effectively, $r \sim 1$) within a moving finger of finite width, and eventual transition to fluctuations with a scale of $t^{5/4}$ (effectively, $r < 1$). For finite L, this transition occurs at $r^*(L) < 1$. However, in the thermodynamics limit $L \to \infty$, the transition value $r^*(L) \to 1$ because the random depositions would cover only a finite part of the lattice. This implies that the KPZ class (at least in 1D) is an unstable point of the dynamics that occurs only at $r = 1$ if L is infinite.

Discussion. We numerically and analytically studied a model of interface growth with memory. The introduction of an overall reduction in propensity driven by local processes, e.g., degradation and diffusion, induces an autonomous decay in propensity at each site. This decay is balanced by local deposition, e.g., local production of cyclic AMP from an activated cell, whose effect increases the propensity for deposition at sites in the vicinity of the recently deposited ones. The uniform decay in propensity is important as it

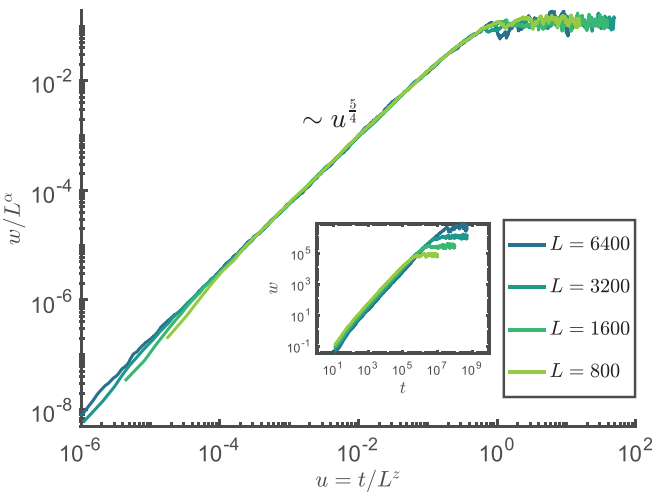

FIG. 4. Interface width w as a function of time for $r = 0.5$ and systems of different lengths L. The time axis is scaled by $L^z = L^2$, and the width axis is scaled by $L^{\alpha} = L^2$, which achieves the collapse of all curves. The data come from averaging over 20 independent runs for all L except $L = 6400$, which used 5 independent runs. The inset shows the bare width as a function of the bare time.

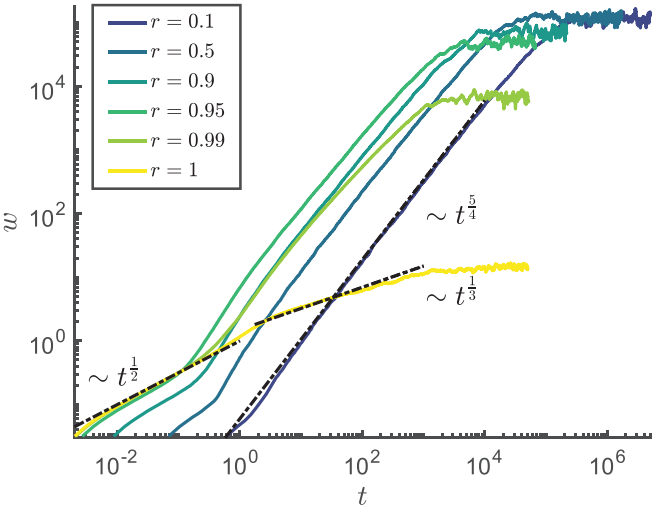

FIG. 5. Interface width w as a function of time for system size $L = 10^3$ and different propensity decay constants r. The growth exponent changes from the KPZ value of $\beta = 1/3$ to the BDM value $\beta = 5/4$ as the propensity decay rate r deviates from $r = 1$. For $r = 1$ and for very small times, the width exhibits the Poisson scaling with $\beta = 1/2$.

limits the interface growth to small randomly moving regions where growth is possible. The introduction of memory—an additional dynamical variable π—changes the order of the dynamics and breaks the temporal locality of the deposition process, so that deposition at the current time is dependent on the history of prior deposition events. This leads to the emergence of a new size exponent γ, which captures the random walk nature of the deposition process at long times, and to changes in the values of the growth exponent ($\beta = 5/4$) and the roughening exponent ($\alpha = 2$). These exponents result in a new scaling law, $z = \frac{\alpha+\gamma}{\beta} = 2$, which generalizes the classical scaling law $z = \alpha/\beta$. In other words, BDM is a surface growth process that does not belong to the KPZ or EW universality classes and their various well-known modifications [13–19]. This is because our novel class breaks spatial translation symmetry by allowing sites to have different probabilities of receiving a deposition.

While our model was inspired by biological systems, it remains to be seen if the discovered universality class is relevant to them. In order to verify this, it might be easier to introduce and study a similar memory-enabled extension of the Eden growth model [6,20]. Further, it is then necessary to explore empirically large spatiotemporal scales that are beyond the typical scales probed in current experiments to test our predicted exponents. We hope that such experiments will provide exciting new insights into interface growth phenomena.

Acknowledgments. The authors thank Fereydoon Family, and I.N. additionally thanks Mehran Kardar for useful discussions. This work was supported in part by the NSF under Grants No. 2010524 and No. 2014173 and by the Simons Foundation Investigator award, Grant No. 827661.

Appendix: Deriving the propensity recursion relation. The dynamics of the propensity in any particular realization of the interface growth are complex. This is largely because the propensity is concentrated, typically, in a small region of the lattice. For our subsequent analysis, we are interested precisely in the typical number of active sites, over which the propensity is large after N depositions. We approximate the number of such significant propensity sites by the total propensity over the whole lattice, averaged over realizations of the process. For the realization j, let $\{\pi_{1,j}(N), \ldots, \pi_{L,j}(N)\}$ denote the propensity on sites $1, \ldots, L$ after N depositions. We now define the total lattice propensity as $\Pi_j^{\text{tot}}(N) = \sum_{\ell=1}^{L} \pi_{\ell,j}(N)$. For this realization, the probability that site k receives the $N+1$st deposition is then $\frac{\pi_{k,j}(N)}{\Pi_j^{\text{tot}}(N)}$. If this occurs, then the total propensity of realization j at deposition $N+1$, conditional on the last deposition being at site k, is

$$\Pi_{k,j}^{\text{tot}}(N+1) = 3 + r \sum_{\substack{\ell \notin \{k,k\pm1\} \\ 1 \leqslant \ell \leqslant L}} \pi_{\ell,j}(N). \tag{A1}$$

Averaging this quantity over the probability of the $N+1$st deposition at site k, we obtain

$$\begin{aligned}
\Pi_j^{\text{tot}}(N+1) &= \sum_{k=1}^{L} \Pi_{k,j}^{\text{tot}}(N+1) \frac{\pi_{k,j}(N)}{\Pi_j^{\text{tot}}(N)} = \sum_{k=1}^{L} \left(3 + r \sum_{\substack{\ell \notin \{k,k\pm1\} \\ 1 \leqslant \ell \leqslant L}} \pi_{\ell,j}(N) \right) \frac{\pi_{k,j}(N)}{\Pi_j^{\text{tot}}(N)} \\
&= 3 + r \sum_{k=1}^{L} \left[\Pi_j^{\text{tot}}(N) - \pi_{[(k-1+L) \bmod L]+1,j}(N) - \pi_{k,j}(N) - \pi_{k+1,j}(N) \right] \frac{\pi_{k,j}(N)}{\Pi_j^{\text{tot}}(N)} \\
&= 3 + r\Pi_j^{\text{tot}}(N) - r \sum_{k=1}^{L} \frac{\pi_{k,j}^2 + 2\pi_{k,j}\pi_{[(k-1+L) \bmod L]+1,j}}{\Pi_j^{\text{tot}}(N)}.
\end{aligned} \tag{A2}$$

Since there are no special sites for ensemble quantities, the ensemble average $\pi(N) \equiv \langle \pi_{k,j}(N) \rangle_{\text{ens}} \equiv \lim_{M\to\infty} \frac{1}{M} \sum_{j=1}^{M} \pi_{k,j}(N)$ is independent of the site k. Consequently, the ensemble average of the total lattice propensity can be related to a site- and ensemble-averaged propensity on a single site:

$$\left\langle \Pi_j^{\text{tot}}(N) \right\rangle_{\text{ens}} \equiv \sum_{k=1}^{L} \langle \pi_{k,j} \rangle_{\text{ens}} \equiv L\pi(N). \tag{A3}$$

Now, averaging Eq. (A2) over propensity configurations, we see that

$$\left\langle \Pi_j^{\text{tot}}(N+1) \right\rangle_{\text{ens}} = 3 + rL\pi(N) - r \left\langle \sum_{k=1}^{L} \frac{\pi_{k,j}^2(N) + 2\pi_{k,j}(N)\pi_{[(k-1+L) \bmod L]+1,j}(N)}{\Pi_j^{\text{tot}}(N)} \right\rangle_{\text{ens}}. \tag{A4}$$

We now assume that fluctuations on nearby sites are uncorrelated so that expectations of products can be approximated as products of expectations. There is little *a priori* reason for this assumption, and we verify its quality *a posteriori* by comparing to simulations. Similarly, we will make another approximation, verified *a posteriori*, that fluctuations in the total propensity are small compared to the mean total propensity, so that the total propensity stays away from 0 (this is because the propensity has to be 1 for a minimum of three sites, which always results in a strictly positive propensity sum). Approximating the average of the ratio by the ratio of the averages ($\langle \frac{x}{y} \rangle \approx \frac{\langle x \rangle}{\langle y \rangle}$) and the average of the product by the

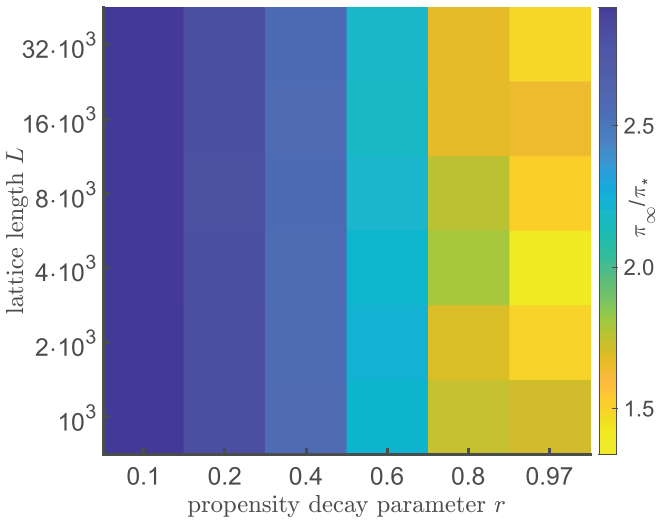

FIG. 6. The ratio π_∞/π_* vs the propensity decay parameter r and the lattice length L. π_∞ is calculated by averaging $\pi(N) = \frac{1}{L}\sum_{\ell=1}^{L}\pi(\ell,N)$ over 30 realizations and then time averaging over N in the steady state.

product of the averages ($\langle xy\rangle \approx \langle x\rangle\langle y\rangle$) [21], we obtain the term

$$\left\langle \sum_{k=1}^{L} \frac{\pi_{k,j}^2(N) + 2\pi_{k,j}(N)\pi_{[(k-1+L) \bmod L]+1,j}(N)}{\Pi_j^{\rm tot}(N)} \right\rangle_{\rm ens} \tag{A5}$$

$$\approx \sum_{k=1}^{L} \frac{\left\langle \pi_{k,j}^2(N) + 2\pi_{k,j}(N)\pi_{[(k-1+L) \bmod L]+1,j}(N)\right\rangle_{\rm ens}}{\left\langle \Pi_j^{\rm tot}(N)\right\rangle_{\rm ens}} \tag{A6}$$

$$\approx \sum_{k=1}^{L} \frac{\pi^2(N) + 2\pi(N)\pi(N)}{L\pi(N)} = \sum_{k=1}^{L} \frac{3\pi(N)}{L} = 3\pi(N). \tag{A7}$$

Using this approximation and Eq. (A4), we obtain

$$\left\langle \Pi_j^{\rm tot}(N+1)\right\rangle_{\rm ens} \approx 3 + r(L-3)\pi(N). \tag{A8}$$

To close this relation, we notice that the site-averaged and realization-averaged total propensity is

$$\left\langle \Pi_j^{\rm tot}(N+1)\right\rangle_{\rm ens} = \left\langle \sum_{\ell=1}^{L} \pi_{\ell,j}(N+1)\right\rangle_{\rm ens} = L\pi(N+1), \tag{A9}$$

and therefore

$$\pi(N+1) \approx \frac{1}{L}[(L-3)r\pi(N) + 3]. \tag{A10}$$

The analysis above makes a lot of approximations, some more justified than the others. Thus, it is important to verify the obtained result independently. For this, we compare the steady state π_* of the recursion relation with our approximations, Eq. (A10), (see the next section for its derivation) to the steady state π_∞ of the ensemble average $\langle\pi(N) = \sum_{\ell=1}^{L}\pi(\ell,N)\rangle$, obtained through numerical simulations. Figure 6 shows that $\pi_\infty = c_{r,L}\pi_*$, where $c_{r,L}$ is an $\mathcal{O}(1)$ factor.

We emphasize that, for our analysis, we only need an order of magnitude estimate of the average propensity, and hence the propensity finger width, which allows us to set the correct scale for how long it takes to deposit a layer of particles in the active part of the system. Discrepancies $\mathcal{O}(1)$ only lead to redefining the scale of time, but not its dependence on the system parameters.

Solving the propensity recursion relation. Multiplying the recursion relation, Eq. (8), by the summing factor $(\frac{L-3}{L}r)^{-N-1}$ and summing from $n = 0$ to $n = N-1$, we obtain a telescoping sum, which evaluates to

$$\pi(N) = \pi(0)\left(\frac{L-3}{L}r\right)^{N-1} + \frac{3}{L}\sum_{n=0}^{N-1}\left(\frac{L-3}{L}r\right)^{n}. \tag{A11}$$

Rewriting the first term of the above expression and the result of the remaining geometric sum in the exponential form yields

$$\pi(N) = \left(\frac{L}{(L-3)r} - \frac{3}{L-(L-3)r}\right)e^{-N\ln\left(\frac{L}{(L-3)r}\right)} + \frac{3}{L-(L-3)r}. \tag{A12}$$

From the first term, we obtain the propensity decay timescale

$$N_{1/e} = \frac{1}{\ln\left(\frac{L}{(L-3)r}\right)} \approx \frac{1}{\ln\left(\frac{1}{r}\right)}, \text{ for } L \gg 1. \tag{A13}$$

Thus $\pi(N)$ exponentially decays to

$$\pi_* = \frac{3}{L-(L-3)r} \tag{A14}$$

on the timescale $\mathcal{O}(N_{1/e})$. In the limits $r \to 1$ and $L \gg 1$, the timescale $N_{1/e} \to \infty$. That is, the propensity remains at the fixed value of $\pi \approx 1$ and no decay occurs, consistent with the regular ballistic deposition process.

Computing deposition probabilities. From Eq. (5), we deduce that if site j receives a deposition at step N, then the probability that site i will receive a deposition is

$$\mathcal{P}[i,N+1] = \frac{\pi_i(N+1)}{\sum_{i=1}^{L}\pi_i(N+1)} = \frac{\pi_i(N+1)}{L\pi(N+1)} \tag{A15}$$

$$\approx \begin{cases} \frac{1}{(L-3)r\pi(N)+3}, & \text{for } j-1 \leqslant i \leqslant j+1 \\ \frac{r\pi(N)}{(L-3)r\pi(N)+3}, & \text{otherwise.} \end{cases} \tag{A16}$$

However, for $N \gg \frac{1}{\ln(1/r)}$, the propensity $\pi(N) \approx \pi_* = \frac{3}{L-(L-3)r}$ and the probability of deposition at site i becomes

$$\mathcal{P}[i,N+1] \approx \begin{cases} \frac{1}{3} - \frac{L-3}{3L}r, & \text{for } j-1 \leqslant i \leqslant j+1 \\ \frac{r}{L}, & \text{otherwise.} \end{cases} \tag{A17}$$

As a check, we see that the probability that any site receives a deposition is 1:

$$\sum_{i=1}^{L}\mathcal{P}[i,N+1] = (L-3)\frac{r}{L} + 3\left(\frac{1}{3} - \frac{L-3}{3L}r\right) = 1.$$

Furthermore, using Eq. (A17), we see that

$$\sum_{\substack{j\notin\{i-1,i,i+1\} \\ 1\leqslant j\leqslant L}} \mathcal{P}[j,N+1|i,N] = \frac{L-3}{L}r \approx r \ll 1 \tag{A18}$$

for $r \ll 1$. Therefore, the position x_N of the deposition at step N follows an unbiased random walk in this regime.

Expanding the random walk regime. In practice, the steady-state propensity π_* is not spread out over the entire lattice. Instead $L\pi_* = 3(1 - \frac{L-3}{L}r)^{-1}$ sites have a propensity of almost 1, and the rest of the lattice has an almost 0 propensity. This motivates the choice of the units of time as $t = \eta \frac{N}{L\pi_*}$ shown in Eq. (9) in the main text. In the limit $L\pi_* \ll L$, the propensity process is made of multiple fingers of cumulative size $L\pi_*$, which all are performing random walks. These fingers dynamically merge and split as particles are deposited randomly. This has the effect that, outside these fingers, the probability of a deposition is 0 and hence our dynamical exponents will hold in the significantly larger regime $L\pi_* \ll L$ or, equivalently, $\frac{3}{1-r} \ll L$.

Extracting exponents from data. To estimate the growth exponent β, we compute the mean width $\langle w(N)\rangle = \frac{1}{n}\sum_{i=1}^{n} w_i(N)$ of n realizations of the simulations, where each w_i is the width of a particular realization, evaluated as in Eq. (1). To ensure that the estimated value of the growth exponent remains in the growth regime and is unaffected by crossover effects, we limit the range of time used in the estimation to $N \in [3 \times 10^2, 3 \times 10^4]$. According to Eqs. (11) and (12), the mean width in the growth regime is $\langle w(N)\rangle \sim L^{-\gamma} N^{\beta}$. Therefore, linear regression obtains the slopes β and γ of the plane $\ln w(N) = \beta \ln N - \gamma \ln L + k$ when regressed against $\ln N$ and $\ln L$, respectively. The slopes obtain values of $\beta \approx 1.25 \pm 0.03$ and $\gamma \approx 0.54 \pm 0.09$.

To determine the size of the fluctuations around the estimated value of β for a fixed substrate length L, we use the covariance matrix $\Sigma_{\beta,\Delta}$ of the parameters β and $\Delta = -\gamma \ln L + k$. The covariance matrix is $\Sigma_{\beta,\Delta} \approx R^{-1}(R^{-1})^T \frac{|\vec{e_{\rm res}}|^2}{df}$, where R is the triangular factor from a QR decomposition of the Vandermonde matrix of $\ln(N)$, $\vec{e_{\rm res}}$ is the vector of residuals between the data and the fitting line, and $df = 2$ is the number of degrees of freedom. The quantity $(\Sigma_{\beta,\Delta})^{1/2}_{\beta,\beta}$ provides the standard deviation on β. A similar procedure is followed when we regress on $-\gamma \ln L + k$ against $\ln L$ to find γ and its standard deviation.

To determine the roughening exponent α, we note that $\langle w(t)\rangle \sim L^{\alpha}$ in the saturated regime. To avoid a bias in the estimate of α due to the transition from growth to saturation, we limit the time range used in the estimate to $N \in I_L = [2L^2, 10L^2]$ for lattice length L. For a fixed lattice length L, the width in the saturation regime fluctuates over the interval I_L. In this regime, the mean width is obtained from the relation $w_{\rm sat} = \frac{1}{|I_L|}\sum_{N\in I_L}\langle w(N)\rangle$, where $|I_L|$ is the length of the interval I_L used for the estimate of $w_{\rm sat}$ of the lattice of length L. Using linear regression, the value of the slope of the line $\ln w_{\rm sat} = \alpha \ln L + \lambda$ gives $\alpha \approx 2.0 \pm 0.18$ as seen in Fig. 3, in agreement with analytical results.

[1] A. L. Barabasi and H. E. Stanley, *Fractal Concepts in Surface Growth* (Cambridge University Press, Cambridge, England, 1995).

[2] F. Family, Scaling of rough surfaces: Effects of surface diffusion, J. Phys. A: Math. Gen. **19**, L441 (1986).

[3] M. Kardar, G. Parisi, and Y.-C. Zhang, Dynamic scaling of growing interfaces, Phys. Rev. Lett. **56**, 889 (1986).

[4] L. A. N. Amaral, A. L. Barabási, S. V. Buldyrev, S. Havlin, and H. E. Stanley, New exponent characterizing the effect of evaporation on imbibition experiments, Phys. Rev. Lett. **72**, 641 (1994).

[5] G. Ódor, Universality classes in nonequilibrium lattice systems, Rev. Mod. Phys. **76**, 663 (2004).

[6] F. Family and T. Vicsek, Scaling of the active zone in the Eden process on percolation networks and the ballistic deposition model, J. Phys. A: Math. Gen. **18**, L75 (1985).

[7] C. J. Wang, A. Bergmann, B. Lin, K. Kim, and A. Levchenko, Diverse sensitivity thresholds in dynamic signaling responses by social amoebae, Sci. Signaling **5**, ra17 (2012).

[8] A. Prindle, J. Liu, M. Asally, S. Ly, J. Garcia-Ojalvo, and G. Suel, Ion channels enable electrical communication in bacterial communities, Nature (London) **527**, 59 (2015).

[9] R. Martinez-Corral, J. Liu, G. M. Süel, and J. Garcia-Ojalvo, Bistable emergence of oscillations in growing *Bacillus subtilis* biofilms, Proc. Natl. Acad. Sci. USA **115**, E8333 (2018).

[10] T. A. Witten and L. M. Sander, Diffusion-limited aggregation, Phys. Rev. B **27**, 5686 (1983).

[11] P. Meakin and F. Family, Diverging length scales in diffusion-limited aggregation, Phys. Rev. A **34**, 2558 (1986).

[12] C Evertsz, Self-affine nature of dielectric-breakdown model clusters in a cylinder, Phys. Rev. A **41**, 1830 (1990).

[13] E. Medina, T. Hwa, M. Kardar, and Y.-C. Zhang, Burgers equation with correlated noise: Renormalization-group analysis and applications to directed polymers and interface growth, Phys. Rev. A **39**, 3053 (1989).

[14] S. Das Sarma and P. Tamborenea, A new universality class for kinetic growth: One-dimensional molecular-beam epitaxy, Phys. Rev. Lett. **66**, 325 (1991).

[15] D. E. Wolf and J. Villain, Growth with surface diffusion, Europhys. Lett. **13**, 389 (1990).

[16] Z. Rácz, M. Siegert, D. Liu, and M. Plischke, Scaling properties of driven interfaces: Symmetries, conservation laws, and the role of constraints, Phys. Rev. A **43**, 5275 (1991).

[17] T. Sun, H. Guo, and M. Grant, Dynamics of driven interfaces with a conservation law, Phys. Rev. A **40**, 6763 (1989).

[18] Z. W. Lai and S. Das Sarma, Kinetic growth with surface relaxation: Continuum versus atomistic models, Phys. Rev. Lett. **66**, 2348 (1991).

[19] J. Villain, Continuum models of crystal growth from atomic beams with and without desorption, J. Phys. I (France) **1**, 19 (1991).

[20] M. Eden, A two-dimensional growth process, in *Proceedings of the Fourth Berkeley Symposium on Mathematics, Statistics, and Probability* (University of California, Berkeley, 1961), Vol. 4, pp. 223–239.

[21] These are the zeroth-order Taylor expansions of the expectation value of the random functions xy and x/y, respectively.